To be cited as: J. Phys. Chem. C, 2007, 111 (13), 4946–4955
DOI: 10.1021/jp0665168

Understanding the vibrational and electronic features of Ti(IV) sites in mesoporous silicas by integrated ab initio and spectroscopic investigations

Gloria Tabacchi[a], *Enrica Gianotti*[b], *Ettore Fois*[a*], *Gianmario Martra*[b], *Leonardo Marchese*[c], *Salvatore Coluccia*[b], *Aldo Gamba*[a]

[a]Dipartimento di Scienze Chimiche Fisiche e Matematiche, Università dell'Insubria and INSTM Udr Como, V. Lucini 3, 22100, Como, Italy

[b]Dipartimento di Chimica IFM and NIS-Centre of Excellence, University of Turin, Via P. Giuria, 7 -10125 Torino- Italy

[c]Dipartimento di Scienze e Tecnologie Avanzate and NIS-Centre of Excellence, Università del Piemonte Orientale, via V. Bellini 25/G, 15100 Alessandria, Italy

*Ettore Fois

V. Lucini 3, 22100, Como, Italy

Phone: ++39 031 326218

FAX: ++39 031 326230

E-mail: fois@fis.unico.it

Abstract

Structural and spectroscopic investigations on Ti(IV) centers in different mesoporous silicas are carried out by an integrated experimental and theoretical approach. The combined study has allowed to highlight many features of the tripodal ($(OH)Ti(OSi)_3$) or tetrapodal $Ti(OSi)_4$ Ti(IV) sites present in the silica matrix, the concentration of which may depend on the synthetic approach adopted to obtain the mesoporous Ti(IV)-SiO_2 materials. The study of the effect of silylation on the catalysts and the model systems has allowed, for the first time, to clarify relevant microscopic details of silylated Ti(IV) sites in mesoporous silicas. Ti(IV) centers are found in a tetrahedral arrangement independently on the tripodal, tetrapodal, or silylated structure and their spectroscopic features are found to be tuned by the silica matrices.

Keywords: Ti(IV), mesoporous silica, simulations, FT-IR, DR UV-Vis-NIR, vibrational and electronic spectra, silylation, titanols

1. Introduction

Ti(IV)-containing mesoporous siliceous materials are active catalysts in selective oxidation reactions of hydrocarbons, in particular in olefin epoxidation reactions.[1-3] Recently, these materials were also used as photocatalysts in the direct decomposition of NO into N_2 and O_2.[4]

The catalytic active centers are tetrahedrally coordinated Ti(IV) cations, the presence of which can be inferred by a variety of spectroscopic techniques such as Diffuse Reflectance (DR) UV-Vis, luminescence and EXAFS/XANES.[5-7] Tetrahedral Ti(IV) centers in Ti(IV)-containing zeolites and siliceous mesoporous materials have a typical electronic transition in the 200-220 nm range in the DR UV-Vis spectra.[6,8-11] Bands in similar positions are associated to oxygen to tetrahedral Ti(IV)

charge transfer transitions (LMCT).[12] According to the empirical optical electronegativity theory,[12] the position of the absorption maximum is strictly dependent on the electronic features of the oxygen atoms bonded to Ti(IV) sites, as the higher the electronegativity of the oxygen atoms, the higher the energy of the LMCT transition. The absorption bands of Ti(IV)-containing mesoporous silicas are generally wide and asymmetric towards higher wavelength values revealing a great heterogeneity of Ti(IV) centers. XANES and EXAFS studies of Ti(IV)-grafted MCM-41 have revealed that tetrahedral Ti(IV) sites, composed of a tripodally linked titanol group ($(OH)Ti(OSi)_3$), were abundant on the catalyst surface and that Ti-O-Ti linkages or titanyl (Ti=O) groups were not present.[7] Based on EXAFS studies, [6,13,14] the strong shoulder at 230 nm, always present in the DR UV-Vis spectra of Ti(IV)-based mesoporous silicas, has been assigned to titanol groups.

On the other hand, the simplest Ti(IV) tetrahedral species, molecular $TiCl_4$, shows two absorption bands in the electronic excitation spectrum, both assigned to $^1A_1$ to $^1T_2$ state transitions.[15] Also, tetrakis(trimethylsiloxy) titanium, a four coordinated Ti(IV) cation tetrahedrally surrounded by four $–O-Si(CH_3)_3$ bridges, presents a multiple band UV spectrum in cyclohexane characterized by a complex intense band centered at 214 nm, a shoulder at 240 nm and an absorption edge at about 280 nm. [16] Recent calculations of electronic excitations in model Ti(IV) zeolites determined that a single tetrahedral zeolitic Ti(IV) site presents multiple band absorption profiles, with absorption wavelengths depending on the local geometry of the Ti(IV) center.[17] Such findings, in agreement with a group-theoretical point of view, indicated that associating a single UV-Vis absorption to a single Ti(IV) tetrahedral species in Ti(IV)-zeolites may be misleading. Therefore a precise LMCT band assignment, even in the case of crystalline Ti(IV) sites, is not straightforward.[17]

Indeed, electronic spectra of Ti(IV)-containing mesoporous materials should be characterized by a greater complexity with respect to Ti(IV)-zeolites, due to the presence of various kinds of Ti(IV) centers, characterized by different local geometries, in the amorphous SiO_2 matrix typical of long-range ordered mesoporous silicas. In this context, the use of simulation models based on first

principles computational techniques might be of crucial relevance for a detailed interpretation of spectroscopic data on the basis of the correlation to the underlying microscopic structure of these materials.[18,19]

In this paper, the presence of Ti-OH groups within the pores of MCM-41 and MCM-48 mesoporous silicas will be discussed by combining DR UV-Vis-NIR and FTIR spectroscopies and ab initio calculations. To clarify the nature of OH groups (Si-OH and Ti-OH), Ti(IV) active sites were introduced by one-pot synthesis in MCM-48 and by grafting a Ti(IV) complex onto the inner walls of MCM-41. Both types of Ti(IV) centers, $Ti(OSi)_4$ and $(OH)Ti(OSi)_3$ sites, are always present in Ti(IV)-containing MCM-41 and MCM-48, nevertheless in Ti(IV) grafted samples $(OH)Ti(OSi)_3$ are more abundant than $Ti(OSi)_4$. Furthermore, Ti-MCM-48 and Ti-MCM-41 catalysts were investigated before and after a post-synthesis silylation treatment of the silica surface. The silylation treatment modifies the environment around Ti(IV) sites converting surface OH groups (Ti-OH and Si-OH) into $Ti–OSi(CH_3)_3$ and $Si-OSi(CH_3)_3$ (scheme 1). Besides, atomic level insight on experimental results was gained by investigating the properties and behavior of model Ti(IV) centers in nanometer-thick amorphous silica slabs via first principles approaches.

Scheme 1.

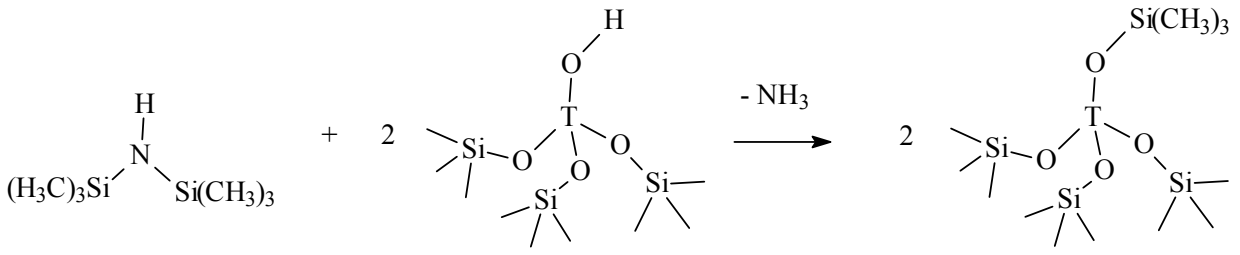

2. Experimental

Ti-MCM-48 samples, prepared by one-pot method, were synthesised as described in literature,[20] using amorphous silica (Aerosil 200, Degussa) as silicon source, cetyltrimethylammonium hydroxide (CTMAOH) as surfactant and titanium tetraethoxide, $Ti(OEt)_4$. The gels were crystallised in Teflon lined stainless-steel autoclaves at 150◦C for 6h, the surfactant was removed by heating at 550°C under continuous flow of N_2 for 1 h followed by calcinations in a flow of O_2 (300 cc/min).

Titanocene dichloride [$TiCp_2Cl_2$] complex was used to functionalise MCM-41 according to the procedure reported by Maschmeyer *et al.*.[7] The Ti(IV)-complexes were grafted onto the Si-OH surface groups and, after calcination in O_2 at 550°C, Ti(IV) catalytic active centers were obtained.

Before grafting titanium centres, the CTMAB surfactant was removed by heating at 550°C, first under N_2 flow and subsequently under O_2. These catalysts had similar Ti loading of *ca.* 2 wt.%.

The silylation was performed by treating the calcined Ti-MCM-41 and Ti-MCM-48 with a solution of hexamethyldisilazane (HMDS) in toluene at 120 °C for 2 h using a HMDS/SiO_2 ratio of 0.25. The catalyst was filtered, washed with dry toluene and finally dried at 60◦C.

X-ray diffraction (XRD) patterns of Ti-MCM-41 and Ti-MCM-48 (before and after silylation treatment) were obtained on a Philips (PW1830) operating with Cu-K_α radiation.

FTIR spectra of self-supporting wafers of the samples were recorded with a Bruker IFS28 spectrometer at a resolution of 4 cm^{-1}. Diffuse Reflectance UV-Vis-NIR spectra were collected by a Perkin Elmer (Lambda 900) spectrometer equipped with an integrating sphere attachment.

All the samples were outgassed at 250°C for 2h to eliminate adsorbed water before spectroscopic measurements, using specially designed cells which were permanently connected to a vacuum line (residual pressure $<10^{-5}$ Torr).

3. Computational methods and models

Simulations were performed on ~1 nm thick silica slabs containing isolated Ti(IV) sites. Each model layer presents two surfaces parallel to the *xy* plane and exhibits a different kind of Ti(IV) site, namely a tetrapodal (Q4), a tripodal (Q3), a bipodal (Q2) or a silylated (Q3S) Ti(IV) center. In addition, an all-silica slab has been modelled as a reference. The simulated layers were designed in such a way to approximately reproduce the experimentally determined smallest wall thickness in porous silicas in a slab geometry with periodic boundary conditions. The Ti(IV) content in the adopted model systems (4.6% wt.) is higher than in the catalyst samples because a closer approximation of their actual Ti-loading would have required larger computational costs. However, all models contained only an isolated Ti(IV) site. Slabs were built in a three dimensional periodic simulation cell of 10.04 × 10.04 × 17 $Å^3$. The cell dimensions in the *x,y* plane were determined by optimization of the cell parameters, while a vacuum region of about 0.7 nm was added along *z* in order to minimize inter-surfaces interactions. The models here adopted do not reproduce the curvature of the MCM-41 or MCM-48 inner walls. However, previous studies performed on similar nanometer-thick all-silica layers provided results in fair agreement with available spectroscopic data, thus validating the adopted model. [18,19]

The electronic structure of the simulated systems was calculated by Density Functional Theory (DFT) approaches, using a plane waves (PW) basis set with a 60 Ry cutoff, and the gradient corrected approximations of Becke and Perdew for the exchange and correlation energies respectively.[21,22] Only valence electrons were explicitly described, while the core electrons were treated via norm conserving pseudopotentials (d-nonlocality for Ti, Si, O and C, and a local pseudopotential for H).[23,24] Such a computational scheme has been extensively applied to the study of many different phenomena in porous crystalline silicates, including proton transfer events,[25] Brønsted acidity,[26] intracage nitrite to nitrate oxidation,[27] host-guest interactions and stability of low dimensionality structures,[28] and behavior at high temperatures and pressures.[29] In all these cases the

present approach has given results in good agreement both with available experimental data and with results from higher level computational schemes. In particular, recent applications of this approach to Ti(IV)–zeolites[17,30-33] have provided a satisfactory description and atomistic level insight on structural, electronic and vibrational properties of Ti(IV) centers.

Both geometry optimizations and First Principles Molecular Dynamics simulations[34-36] (FPMD) were performed. An electronic fictitious mass of 500 au, a time step of 0.121 fs and a target simulation temperature of 298 K (NVT ensemble) were adopted in the FPMD runs. As experimental atomic positions were not available as input, the starting configuration of the reference all-silica slab, of formula $Si_{16}O_{32}$, was obtained by cutting a slice of ~ 1 nm thickness from a silica glass. First, the slab was equilibrated by classical molecular dynamics simulations with an empirical force field.[37] The unsaturated Si/O atoms were gradually removed by a simulated annealing procedure and by adding water molecules, up to a final unit cell stoichiometry of $Si_{16}O_{32}{\cdot}2H_2O$. Point defects such as dangling bonds or strained bridges (*e.g.* two and three membered rings) were not present in the equilibrated structure. Then, the optimal cell parameters were determined by minimizing the total DFT energy of such a model silica slab (with 90 Ry cutoff) with respect to nuclear positions and cell parameters. The parameters corresponding to the energy minimum ($a = b = 10.04$ Å) were adopted in all the simulations performed in this study. The reference system R, modelling an hydrated silica layer characterized by a surface silanol density of 3.97 SiOH/nm^2, presents four silanol groups on the same surface (Figure 1a). The behavior at room conditions of the reference structure was studied by performing a FPMD run of ~10 ps. The Ti-containing models here adopted were derived from configurations sampled along that trajectory. System Ti-Q3, with stoichiometry $TiSi_{16}O_{34}{\cdot}H_2O$, was built from a configuration characterized by three Si-OH groups at close distance, by removing the hydroxyl protons and "grafting" on the three dangling bonds a Ti-OH species. System Ti-Q4 has unit cell stoichiometry $TiSi_{16}O_{34}{\cdot}H_2O$ and is characterized by a tetrapodal Ti(IV) site and two surface Si-OH groups. It was generated by exchanging the location of Ti with that of a Si in the Ti-Q3 system. System Ti-

Q2, $TiSi_{16}O_{34}\cdot H_2O$, has been obtained from R by removing a water molecule and replacing two hydrogens from vicinal Si-OH groups with a $Ti(OH)_2$ group, *i.e.* forming two geminal titanols. Finally, system Ti-Q3S ($TiSi_{17}O_{34}\cdot H_2O(CH_3)_3$), modelling a silylated Ti(IV) site, was built by replacing the titanol proton in Ti-Q3 by a Si-$(CH_3)_3$ group. The four Ti(IV)-loaded model silica slabs are represented in Fig. 1b-e. The room temperature time evolution of each model system was followed for about 10 ps. Average structural parameters and vibrational spectra were calculated from such trajectories. Vibrational spectra were obtained from partial contributions due to the T-O-T modes,[31] where T represents a Ti or Si atom, calculated from the Fourier transform of appropriate autocorrelation functions.[38] Since in the Car Parrinello technique a fictitious mass is associated with the wavefunction coefficients,[34] the calculated vibrational spectra have to be scaled accordingly.[31,36] Electronic spectra were obtained from the Franck-Condon optical conductivities of configurations sampled along the finite temperature trajectories of the Ti(IV)-containing model slabs. Optical conductivities were calculated by the formula:[39,40]

$$\sigma(\omega) = \frac{2\pi e^2}{3m_e{}^2 \omega V} \sum_{i,j=1}^{N} (f_i - f_j) \left\langle i|\hat{\mathbf{p}}|j \right\rangle^2 \delta\left((\varepsilon_i - \varepsilon_j) - \hbar\omega\right) \quad (1)$$

where $|i\rangle$,$|j\rangle$ are electronic states, ε_i, ε_j electronic eigenvalues, V the cell volume, ω the frequency, f_i, f_j occupation numbers, p the electronic momentum operator and N the total number of states (occupied + empty). Besides the occupied states, 60 empty electronic states were included in the summations. Optical conductivity calculations were performed using a 90 Ry cutoff on geometries obtained using the smaller basis set (60 Ry).

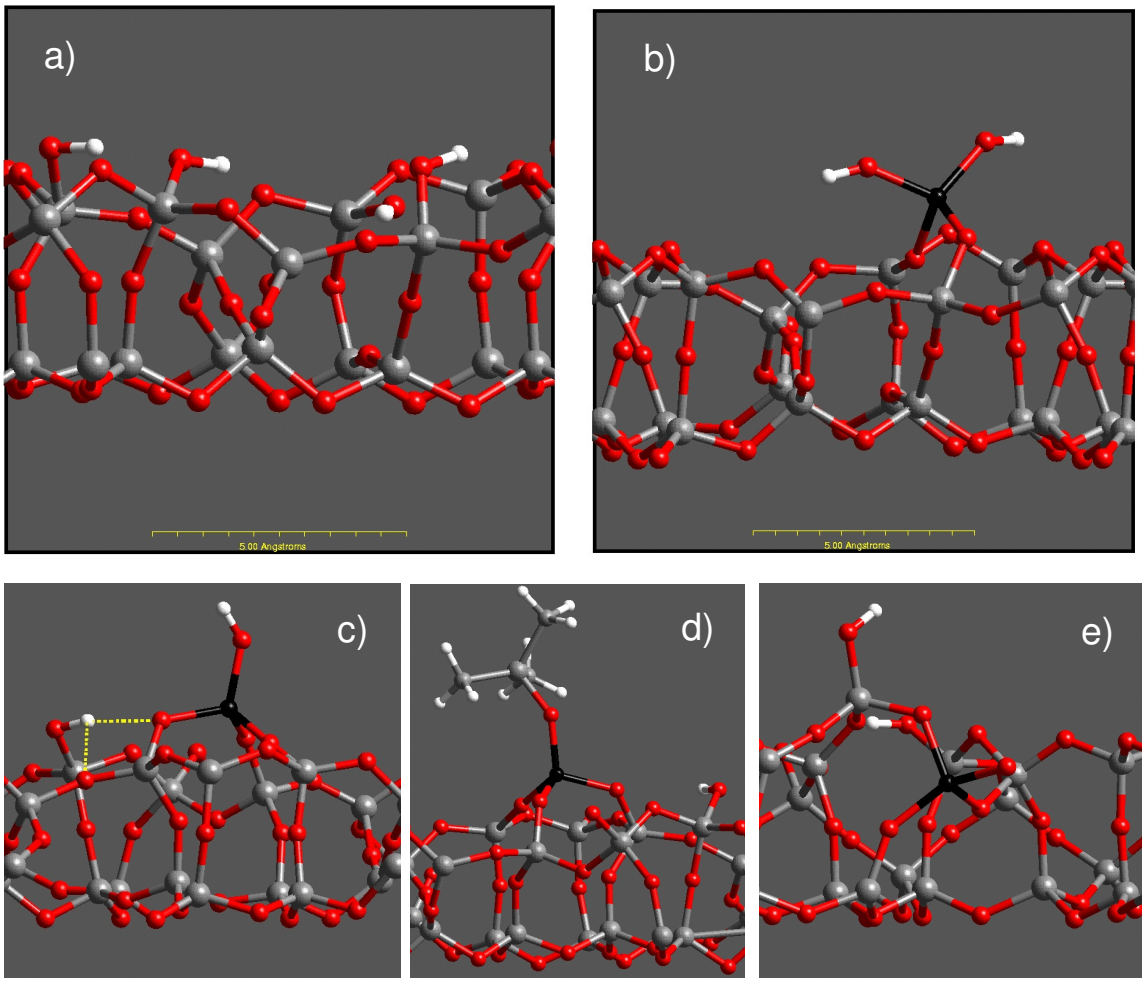

Figure 1. Graphical representation of the model slabs. a) Hydrated silica reference system R; b) Ti-Q2 system (bipodal Ti); c) Ti-Q3 system (tripodal Ti); d) Ti-Q3S (sylilated Ti-Q3 site); e) Ti-Q4 system (tetrapodal Ti). Colour codes: Black: Ti; gray: Si; red: O; white: H. In the Ti-Q3 system hydrogen bonds are evidenced as dashed lines.

4. Results

4.1 Structural characterisation

4.1.1 XRD analysis

The XRD analysis allowed to monitor the structural modification of the MCM-41 and MCM-48 after the introduction of Ti(IV) centres and silylation treatment.

X-Ray diffraction of calcined TiMCM-48, obtained by one-pot synthesis, shows a pattern typical of a material with cubic Ia3d symmetry, with a main (211) reflection at 2.5° and other weaker peaks at higher 2θ values.[41] In the case of Ti-MCM-41 grafted sample, the structural modifications were followed after both the Ti(IV) grafting and the silylation treatments. The hexagonal network of mesopores typical of P6mm structure with a main (100) peak at 2.34° (2θ value) and other two weaker signals at higher 2θ values,[42] are still clearly observed after the Titanocene grafting onto the walls of MCM-41 and the subsequent calcinations.

Upon silylation, the structures kept similar unit cell parameters to the calcined samples in both Ti-MCM-48 and Ti-MCM-41.

4.1.2. Simulations results on the model layers

The average structural properties calculated for the Ti-containing model layers are compared with the ones obtained for the reference all silica layer R. Calculated average Ti-O distances and O-T-O angles (T= Si, Ti) are reported in Table 1.

Table 1. Room temperature average geometrical parameters[a] of the tetrahedral units calculated for the model systems. Distances in Å, angles in degrees, tetrahedra volumes in Å^3.

	R	Ti-Q2	Ti-Q3	Ti-Q3S	Ti-Q4
Si-O	1.647 (0.032)	1.646(0.035)	1.647 (0.034)	1.646 (0.028)	1.647 (0.034)
O-Si-O	109.5 (3.5)	109.5 (3.3)	109.4 (3.3)	109.4 (3.2)	109.4 (3.3)
V_{SiO4}	2.244 (0.062)	2.220(0.063)	2.241 (0.062)	2.238 (0.054)	2.245 (0.061)
Ti-O	-	1.820(0.029)	1.824 (0.028)	1.826 (0.028)	1.833 (0.031)
O-Ti-O	-	109.4 (5.4)	109.3 (4.7)	109.2 (6.0)	109.0 (6.0)
V_{TiO4}	-	3.044(0.070)	3.046 (0.065)	3.032 (0.074)	3.034 (0.094)

[a]Calculated standard deviations are reported in parenthesis, they represent an estimation of the amplitude of the fluctuations due to thermal motion.

In all the simulated systems, the average O-Si-O angle is very close to 109.4°, even though deviations from the ideal tetrahedral geometry along the FPMD runs were observed. Interestingly, all systems exhibit a nearly identical average internal geometry of the Si tetrahedral units, with an average Si-O bond length of 1.646 Å, and also very similar values of the SiO_4 tetrahedron average volume. Moreover, in line with the results reported in Ref. 19, such an average SiO_4 geometry, calculated for quasi 2-dimensional layers, is very close to that found in standard 3-dimensional systems (i.e. bulk amorphous SiO_2 or zeolites). Differences among the Ti-containing layers are however found by inspecting the average internal geometry of the TiO_4 tetrahedron, as expected on the basis of the different types of Ti(IV) species here modelled. The average Ti-O distance gradually increases in passing from the Ti-Q2 to the Ti-Q4 system. Remarkably, the average TiO_4 geometry is very similar in Ti-Q3 and Ti-Q3S systems. The TiO_4 unit in the Ti-Q4 system is the one characterized by the longest Ti-O average bond length, the largest deviation of the O-T-O angle from the ideal tetrahedral geometry and by the largest room temperature fluctuations.

The calculated distribution of the Ti-O-X angles, where X can be Si, H or $Si(CH_3)_3$ depending on the model systems, are shown in Fig. 2. In Ti-Q3 two distinct peaks are found, at 126° and 161°, which are typical values of T-O-T angles in silicates. In the Ti-Q2 system the two Ti-O-H angles are characterized by a broad distribution with a maximum at 122° (Fig 2b), while the Ti-O-Si angles show a narrower distribution centered at 129° (Fig 2c). The Ti-O-H distribution is broader than the Ti-O-Si one because of the higher mobility of Ti-O-H with respect to a standard T-O-T framework bridge. In Ti-Q3S, the Ti-O-$Si(CH_3)_3$ angle distribution shows a broad peak at 149°, while the maxima due to the three Ti-O-Si bridges, which are connected to the polymeric network, are found at values (125° and 162°) very similar to those found in the Ti-Q3 system (Fig 2c). Finally, three contributions may be distinguished in the Ti-O-Si angle distribution in Ti-Q4, a main peak at 126°, an intense shoulder at 138° and a weaker one at 109° (Fig 2a). Such a distribution, different from those shown by the other model Ti(IV) sites, is typical of a system containing strained Ti-O-Si linkages.

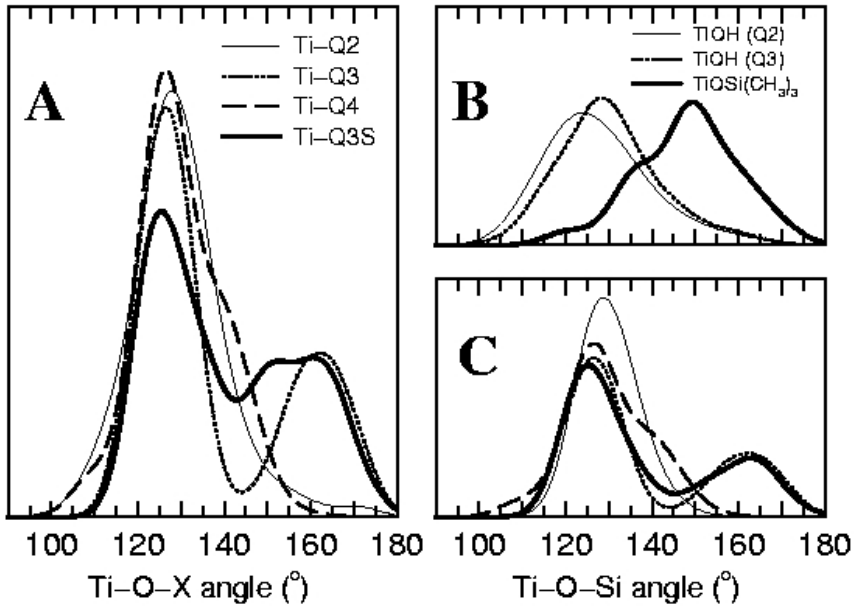

Figure 2. Panel A: Total distribution of the Ti-O-X angles (where X = Si, H or $Si(CH_3)_3$) calculated for the four Ti-containing model slabs. Panel B: calculated distributions of the Ti-O-H angles in the Ti-Q2 and Ti-Q3 systems, and of $Ti\text{-}O\text{-}Si(CH_3)_3$ in Ti-Q3S. Panel C: calculated distribution of the Ti-O-Si angles (line codes as in panel A).

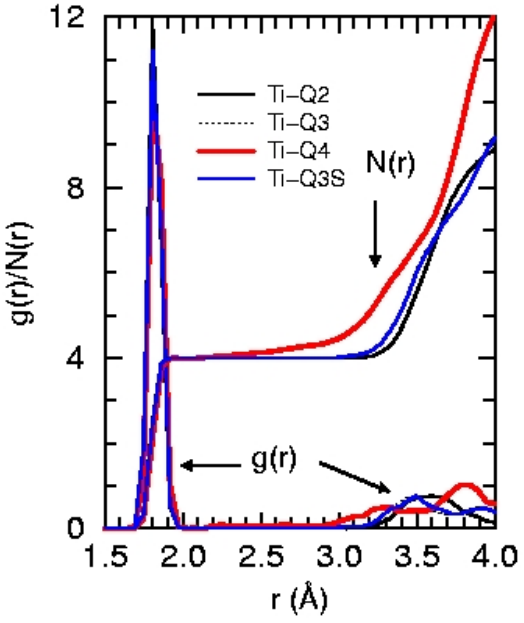

Figure 3. Ti-O pair correlation function g(r) and running coordination number N(r) calculated for the Ti-containing model systems.

Equilibrium structural information can be gathered from pair correlation functions, g(r). The first peak of the Si-O g(r) (not shown) is found at 1.637 Å for all the model layers, as expected for a SiO_2-based system. The Ti-O g(r) and running coordination number N(r) calculated for the four slabs are reported in Fig 3. The first peak of the Ti-O g(r)'s is found at 1.806 Å in all the simulated systems. Such a value corresponds to the most probable Ti-O distance. The fact that the peak position does not change among the four systems while the average Ti-O distance does vary can be rationalized by taking into account the differences in the local environment occupied by Ti(IV) in the various model slabs. The peak position and the very similar value of the average O-Ti-O angles, indicate a close tetrahedral geometry of TiO_4 in the four model systems. However, in the Ti-Q4 slab, a fifth oxygen is found closer to Ti than in the other Ti-containing slabs, as indicated by the corresponding g(r) and N(r). In Ti-Q4, Ti reaches a coordination number of 4.5 at distances slightly lower than 3 Å, while in the other three models the Ti(IV) center remains strictly tetracoordinated in that range. This finding, along with the distribution of the Ti-O-Si angles above discussed, suggests that the Ti-Q4 model system is the one showing the most stressed Ti environment. This is also confirmed by the greater difference between the average (1.833 Å) and the most probable Ti-O distance (1.806 Å) found for the model tetrapodal Ti(IV) site, and might be associated to a not fully relaxed Ti site. Interestingly, the g(r)'s and N(r)'s calculated for the Ti-Q3 and Ti-Q3S slabs are nearly identical, indicating a strong similarity of the average structure of the Ti(IV) center in these model systems.

4.2. Vibrational features

4.2.1. FT-IR spectra

Fig.4A reports the FTIR spectra of calcined MCM-41 (curve a), Ti-MCM-41 (curve b) and Ti-MCM-48 (curve c) in the O-H stretching region. In all spectra a sharp band at 3745 cm^{-1} is present

due to the OH stretching vibration of isolated silanol groups. The intensity of this band is lower in Ti-MCM-41 sample (curve b) with respect to pure MCM-41 (curve a) due to the fact that hydroxyls are the locus where the titanocene is anchored. In the spectra of Ti(IV) samples, the band at 3745 cm^{-1} appears more asymmetric in the low wavenumber side; nevertheless from these spectra it is not possible to evidence the O-H stretching mode of Ti-OH groups. In Fig.4B, the FTIR spectra in the 975-770 cm^{-1} region are reported. A strong absorption at 930 cm^{-1}, not present in the case of MCM-41 (curve a), is clearly visible in the spectrum of Ti-MCM-41 (curve b) which is assigned to the asymmetric stretching of Ti-O-X groups (X=Si or H).[43] Also in the case of Ti-MCM-48 (curve c), a signal at ca. 930 cm^{-1}, although with lower intensity, is present. A band in a similar position (960 cm^{-1}) is observed for TS-1, where Ti(IV) sites are coordinated to four siloxy groups rather than to three siloxy and one hydroxyl group.[8]

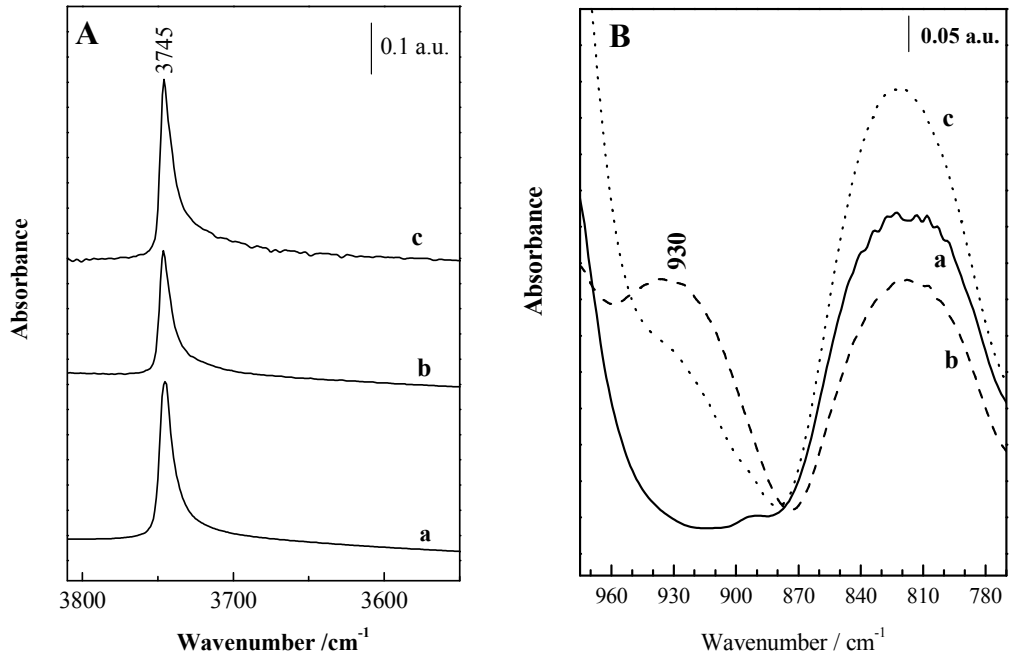

Figure 4 – FT-IR spectra of MCM-41 (curve a), Ti-MCM-41 (curve b) and Ti-MCM-48 (curve c) in the high (Section A) and low (Section B) frequencies region. All the samples were calcined in O_2 at 550°C for 12h.

Fig. 5 shows the FTIR spectra, in the low frequency region, of calcined (curve a) and silylated (curve b) Ti-MCM-41. Calcined Ti-MCM-41 (curve a) exhibits signals at 980 cm^{-1}, due to Si-O stretching mode of Si-OH groups[44,45] and at 940 cm^{-1}, assigned to the asymmetric stretching mode of Ti-O-X (X= Si or H) groups.[8,46] The band at 980 cm^{-1}, after the silylation treatment (curve b), completely disappeared indicating that all Si-OH are converted in Si-O-Si$(CH_3)_3$ groups. This is also confirmed by the disappearance of the band at 3745 cm^{-1} due to the O-H stretching mode of free Si-OH and by the presence of bands at lower frequencies typical of C-H stretching modes of –Si$(CH_3)_3$ groups (reported in the Supporting Information).

The band at 940 cm^{-1}, directly correlated to the Ti(IV) presence, becomes broader and shifts at 950 cm^{-1} after silylation. A signal in similar position is observed on TS-1 where the Ti(IV) sites are considered to be coordinated to four siloxy groups (Ti$(OSi)_4$) rather than to three siloxy and one hydroxyl groups.[8,43,46] This suggests that Ti-OH groups are present and after silylation are converted in Ti-O-Si$(CH_3)_3$ groups. In addition, in the spectrum of silylated sample (curve b), bands at 755, 690 and 620 cm^{-1}, due to the Si-C stretching mode of –Si$(CH_3)_3$ groups, are present.

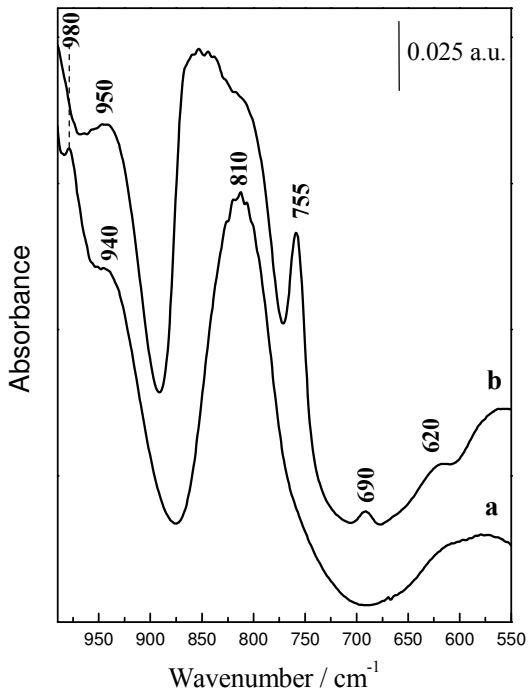

Figure 5. FTIR spectra of TiMCM-41 calcined (curve a) and silylated (curve b). Before the FTIR measure both samples were outgassed at 250°C to remove adsorbed water.

4.2.2. Simulated vibrational spectra.

In the Ti(IV) containing model layers, surface OH groups are present, either as Ti-OH and as Si-OH. In the high wavenumbers region, the DFT calculated OH frequencies are in general red shifted with respect to the experimental values. However, as frequency differences are well reproduced, the relative values are meaningful.[18,31] The Ti-Q3 model system presents one isolated titanol pointing outside the surface ("external" Ti-OH) and one "internal" silanol group involved in hydrogen bonds with the silica network, as shown in Fig. 1c. System Ti-Q4 shows two silanol groups, an "internal" and an isolated "external" one, which, by construction, have structural environments similar to the Ti-Q3 "internal" and "external" groups respectively. In the Ti-Q3 model layer, the calculated OH stretching frequencies are 3673 and 3579 cm^{-1} for the "external" titanol and "internal" silanol groups respectively. In Ti-Q4 the OH frequencies are 3669 ("external") and 3581 cm^{-1} ("internal") (see Fig. 6). The "internal" silanol groups, involved in hydrogen bonds in both systems, show close values of the OH frequency, as expected. However also the isolated "external" Ti-Q4 silanol (3669 cm^{-1}) and Ti-Q3 titanol (3673 cm^{-1}) have very similar frequencies. The extremely close values calculated for "external" OH stretching frequencies are therefore in line with the well-known difficulty in discriminating titanols from silanols in the high frequency region of experimental IR spectra. The geminal titanol groups in the Ti-Q2 system show OH stretching bands in the same range (at 3643 and 3659 cm^{-1}), however at wavenumbers slightly lower than isolated Ti-OH groups.

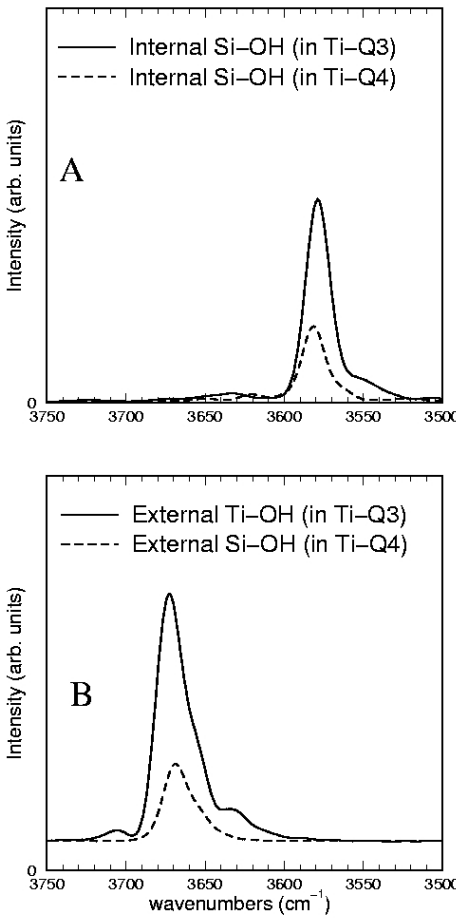

Figure 6. Calculated contributions of the titanol and silanol groups to the OH stretching region of the vibrational spectra of the Ti-Q4 and Ti-Q3 model systems. Calculated spectra were smoothed by using a gaussian of 5 cm^{-1} width. Panel A: contributions of the internal Si-OH groups. Panel B: contributions of the external T-OH groups (T=Si,Ti).

The 1000-750 cm^{-1} region of the vibrational spectra calculated for the model slabs is shown in Fig. 7A, where also the partial vibrational spectra due to the Si-O-Si modes of the R system is reported for comparison. In system R, low-frequency bands (600-400 cm^{-1}) are mainly due to the Si-O-Si bending, while the regions typical of the Si-O-Si symmetric stretching (850-650 cm^{-1}) and Si-O-Si asymmetric stretching (1150-950 cm^{-1}) modes are separated by the so-called silica-window, a semi-transparent region with a minimum here found at 885 cm^{-1}. Such a region is however narrower and less transparent than the silica window in a crystalline system owing to the more

disordered structure of the hydrated silica slab. In this respect, it is worth recalling that the narrowing of the silica window in SiO_2 is strongly correlated with the strain of the SiO_2 polymeric network, moreover in presence of very stressed arrangements of tetrahedra new bands may show up in the silica window.[19] Vibrational spectra are affected by the degree of strain in the modelled amorphous slabs, and a completely relaxed structure is difficult to obtain, especially in one-nanometer-thick layers. This is evident from the calculated spectrum of the reference system R, where the asymmetric T-O-T mode appears at about 960 cm^{-1}. The presence of Ti(IV) centers implies in general a further narrowing of the silica window due to the contributions of the Ti-O-X modes (where, in the present case, O-X = O-H, O-Si and O-Si$(CH_3)_3$). This effect is more pronounced in the case of the simulated Ti-Q4 system, where the region between 870 and 920 cm^{-1} is partially obscured. This result is due to the strain in the Ti(IV) local environment found in the present Ti-Q4 model, as discussed above. Indeed, these bands are absent in the case of simulated zeolitic Ti (Q4) centers[31] (see also Supporting Information). At difference from the Ti-Q4 slab, in the other Ti-containing model systems the width of the semitransparent region is closer to that found in typical IR spectra of mesoporous Ti-silicas. In particular, in passing from Ti-Q3 to Ti-Q3S a narrowing and a blue-shift of the minimum (from 880 to 920 cm^{-1}) is found (Fig 7B), in line with the features observed in the FT-IR spectra of calcined and silylated TiMCM-41 (Fig 4). Moreover, in agreement with experimental spectra, silylation displaces the bands due to the Ti(IV) center towards higher wavenumbers.

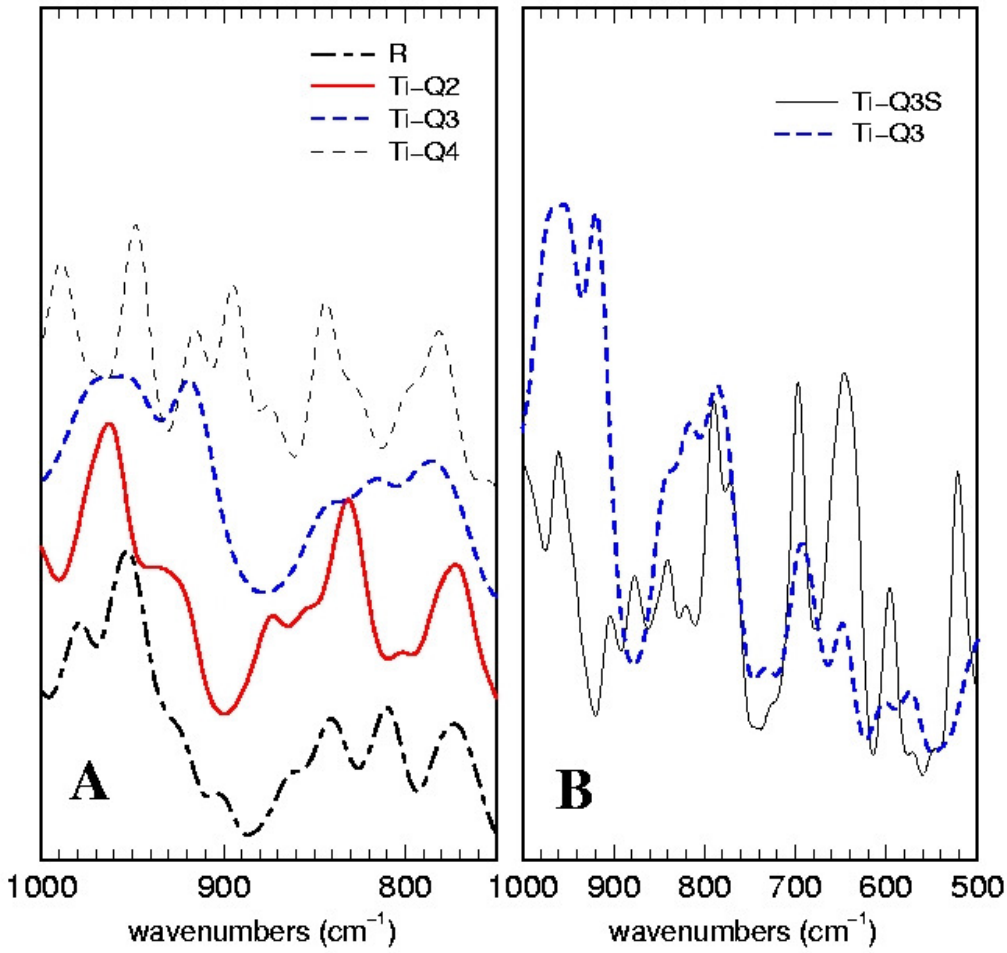

Figure 7. Vibrational spectra calculated for the Ti containing model systems. For system R, only the contribution due to the Si-O-Si modes is reported. Intensity in arbitrary units. Calculated spectra were smoothed by using a gaussian of 5 cm^{-1} width.

With respect to the reference system R, the two Ti "grafted" slabs, namely Ti-Q2 and Ti-Q3, show characteristic features, at 925 and 917 cm^{-1} respectively, due to the Ti-O-X asymmetric stretching modes. Upon silylation, i.e. in passing from the Ti-Q3 to the Ti-Q3S model, the 917 cm^{-1} peak disappears, while a shoulder at 942 cm^{-1} appears in Ti-Q3S. Such modifications could be related to the shift of the 930-940 cm^{-1} feature of calcined Ti-MCM-41 samples (Figure 4 and 5) to 950 cm^{-1} in silylated Ti-MCM-41 (Figure 5). The complex band centered at ~820 cm^{-1} in the Ti-Q3 spectrum is mainly due to the symmetric stretching modes of T-O-T bridges of the silica polymeric

network and corresponds to the broad band found at 810 cm^{-1} in the FTIR spectrum of calcined Ti-MCM-41.

In the low frequency region, the Ti-Q3S simulated vibrational spectrum (Fig 7B) shows two peaks, at 520 and 648 cm^{-1}, due to the O-Si-C symmetric and asymmetric stretching respectively, which also couple with the Ti-O-Si$(CH_3)_3$ modes, as indicated by partial spectra (reported in the Supporting Information). The higher wavenumber peak may be associated with the weak band found at about 620 cm^{-1} in the FTIR spectrum of silylated Ti-MCM-41 (Fig 4). The bands at 696 and 770 cm^{-1}, corresponding to the peaks at 690 and 755 cm^{-1} in the FTIR spectrum of silylated Ti-MCM-41, arise from combinations of symmetric and asymmetric O-Si-C modes, which do not couple with Ti-O-Si$(CH_3)_3$, and should therefore be mainly due to the Si-C bonds. The three Ti-O-Si bridges of the polymeric network are responsible of the shoulder at 942 cm^{-1}, which might correspond to the group of peaks centered at 950 cm^{-1} in the FT-IR spectrum of silylated Ti-MCM-41. Also the low intensity peak at ~900 cm^{-1} is attributed to such Ti-O-Si bridges on the basis of comparison of selected partial spectra. Finally, the band at ~880 cm^{-1} is mainly due to O-Si-C stretching modes. Such a band, that could be considered the main responsible of the narrowing of the silica window in the silylated system, may be identified with the high intensity multiple peaks band at 850-860 cm^{-1} in the experimental FT-IR spectrum.

4.3 Electronic features

4.3.1. DR UV-Vis-NIR spectra

In Fig 8, the DR UV-Vis spectra of calcined and silylated Ti(IV) centres introduced by one-pot synthesis in MCM-48 and by grafting in MCM-41 are reported.

The absorption maximum of calcined Ti-MCM-41 (curve a) is centred at 215 nm, asymmetric towards higher wavelength; in particular a strong shoulder at ~ 230 nm extending up to 270 nm is

visible. Bands in this range are due to LMCT transitions of isolated Ti(IV) sites in tetrahedral coordination.[6,8-11] After silylation treatment (curve b), the absorption band appears sharper and shifted at lower wavelength (ca. 210 nm). This behavior might be explained considering that the electronic environment around Ti(IV) sites in $(OSi)_3$ Ti–$OSi(CH_3)_3$ species formed upon silylation is similar to that of $Ti(OSi)_4$ centers present in TS-1 zeolite, producing a signal at 210 nm.[8] Based on these results, we suggest that Ti-OH groups are responsible for the electronic absorptions at higher wavelength (220-230 nm range) always present in Ti(IV) containing calcined mesoporous silica spectra.

A close result is obtained in the DR UV-Vis spectra of Ti-MCM-48. In fact, the calcined sample (curve c), beside the band with a maximum at around 210-215 nm due to tetrahedral Ti(IV) centers, shows a strong shoulder centred at ~ 230 nm. This feature is removed by silylation treatment (curve d) and the band became sharper, confirming that, also on this sample, $Ti(OSi)_3OH$ are present and are responsible for the absorption signal at higher wavelength values with respect to that of $Ti(OSi)_4$ species. The absorption maximum of calcined Ti-MCM-48 (curve c) is closer to that of TS-1.

The erosion of the features at higher wavelength of the UV band upon silylation is more evident on the Ti-MCM-41 sample. We remind that Ti-MCM-41 is synthesised grafting a Ti(IV) complex onto the inner walls of MCM-41 and after calcination tripodally linked titanol groups ($(OH)Ti(OSi)_3$) are the most abundant species; whilst in Ti-MCM-48, Ti(IV) sites are introduced by one-pot synthesis and thus the TiOH concentration should be lower because most of Ti(IV) sites are present as $Ti(OSi)_4$ species.

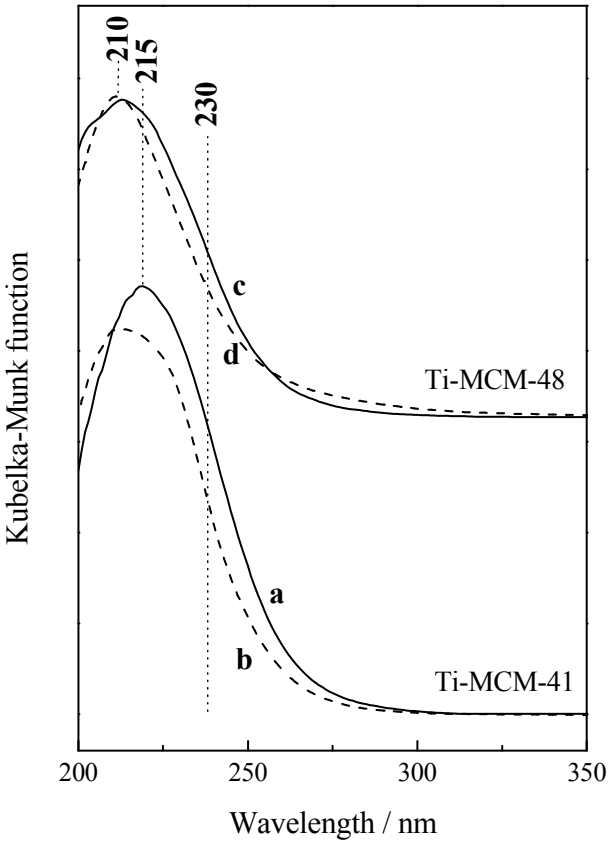

Figure 8. DR UV-Vis spectra of calcined Ti-MCM-41 (curve a), silylated Ti-MCM-41 (curve b), calcined Ti-MCM-48 (curve c) and silylated Ti-MCM-48 (curve d).

The silylation effect on hydroxyl groups can be monitored also by DR NIR spectroscopy. In Fig. 9, NIR spectra of calcined and silylated Ti-MCM-41 and Ti-MCM-48 samples are reported. Two sharp bands at 1370 and 2210 nm are present in calcined samples (curves a and c), assigned to the first overtone of the stretching mode and to a combination of stretching and bending modes of isolated silanol groups.[5,13,14,47] Sharper bands in similar position are also present in the NIR spectra of MCM-41 and MCM-48 systems,[5,47] this effect is due to the larger heterogeneity of the hydroxyl population on the Ti(IV) samples, where Si-OH are present together with Ti-OH and OH groups close to Ti(IV) Lewis acid sites. Upon silylation (curves b and d), both the bands due to isolated silanols disappear and overtone and combination bands of CH_3 groups appear in the 1650-1800 and 2100-2450 nm range respectively. This is an evidence that the OH population drastically decreased and that almost all isolated hydroxyl groups have reacted with HDMS, leading to trimethylsilyl

groups anchored on the Ti-MCM-41 and Ti-MCM-48 silica surfaces, confirming the effectiveness of silylation treatment. In addition, the NIR spectra of calcined samples (curves a and c) evidence a different intensity of the bands due to isolated silanols, in particular the bands of Ti-MCM-41 are less intense compared to those of Ti-MCM-48. This is due to the fact that in Ti-MCM-41, the isolated silanol groups are the locus on which the Ti(IV) grafting occurs and then their population is lower.

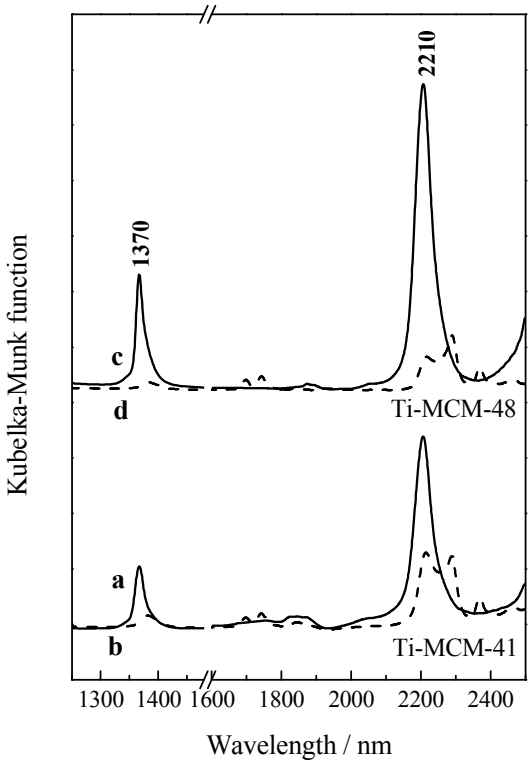

Figure 9. DR NIR spectra of calcined Ti-MCM-41 (curve a), silylated Ti-MCM-41 (curve b), calcined Ti-MCM-48 (curve c) and silylated Ti-MCM-48 (curve d).

4.3.2. Simulated electronic spectra.

In Ti(IV)-loaded mesoporous silicas the analysis of electronic excitation spectra may be complicated by the simultaneous presence of different types of Ti(IV) sites in the amorphous matrix. Comparison with the electronic excitation properties of Ti(IV) sites in a crystalline system may help in providing a solid background on which such investigations should be based.

Geometry optimizations have been performed on model Ti-zeolites, namely Ti-offretite (Ti-Off) and Ti-sodalite (Ti-Sod). Calculations of the electronic excitations can be performed via a TD-DFT approach[48] on clusters derived from the optimized periodic zeolite structure, as shown in Ref. 17. In the case of Ti-Off, three main bands were found at 187, 216 and 233 nm, while in Ti-Sod the calculated absorption maxima are located at 197, 216 and 238 nm.[17] Both TD-DFT spectra and DFT optical conductivities calculated for such zeolitic Ti-Q4 centers with periodic boundary conditions (Eq. 1) are shown in Fig 10. DFT predicted excitation wavelengths (197, 218 and 235 nm for Ti-Off; 195, 225 and 242 nm for Ti-Sod) are fairly in line with results from the more accurate TD-DFT technique. Moreover, the optical conductivities of the corresponding reference all-silica model systems have absorption edges below ~ 180 nm, thus indicating that bands in the λ >180 nm region of the simulated electronic spectra are indeed due to Ti(IV). On the basis of these benchmark calculations, simulation of the electronic excitations of the Ti(IV) centers in the model amorphous slabs has been carried out by calculating DFT optical conductivities.

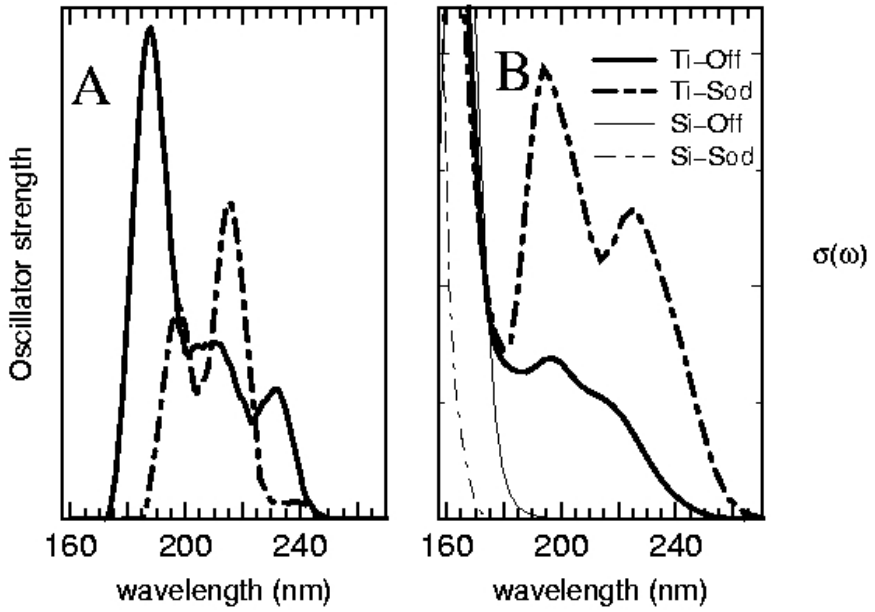

Figure 10. Panel A: TDDFT oscillator strengths calculated for tetrapodal Ti clusters derived from the Ti-Off (solid line) and Ti-Sod (dashed line) optimized structure respectively. Panel B: DFT

optical conductivities calculated for the Ti-Off and Ti-Sod systems. The optical conductivities calculated for model all-silica offretite and sodalite have also been reported for comparison.

Electronic excitation spectra of the four Ti-containing silica slabs calculated by sampling the optical conductivity along the corresponding FPMD trajectories are shown in Fig.11. The Ti-silylated system, besides two features at 204 and 222 nm, shows a broad tail characterized by two peaks, at 252 and 275 nm respectively, not present in the electronic spectra of the other Ti-slabs. Indeed, the Ti-Q4 spectra shows absorptions at 206, 222, and 242 nm, the Ti-Q2 one is characterized by bands at 197 and 212 nm and a shoulder at 230 nm, while the electronic excitations of Ti-Q3 are found at 200, 217 and 235 nm. All these values are in line with typical absorption wavelengths of tetrahedral Ti(IV) centers, as well as with the absorption bands position in the DR UV-Vis spectra of Ti-containing calcined mesoporous silicas (Fig 8). The feature at 242 nm in the Ti-Q4 excitation spectrum might be due to the presence of a strained arrangement of tetrahedra in this particular model system. Remarkably, the intensity of the Ti-Q3S simulated spectrum is significantly lower with respect to the other systems in the region between 220 and 240 nm. This finding is in agreement with the experimental spectra showing an erosion of the absorption profile at ~230 nm after silylation for both Ti-MCM-41 and Ti-MCM-48. Interestingly, the appearance of a high-wavelength tail in the calculated spectra upon "silylation" of the model Ti(IV) center is also observed in the UV-Vis spectra in passing from calcined to silylated Ti-MCM-48, but is not found in the Ti-MCM-41 case. Such a result led to a closer inspection of the electronic properties of the Ti-Q3S system. The contributions to the optical conductivity of two representative structures, selected from a set of configurations evenly sampled along the Ti-Q3S trajectory, are shown in Fig. 11. Each contribution is characterized by different peak positions and intensities due to differences in the local geometry of the Ti(IV) center. Such a behavior, also found in the other model systems, is particularly evident in the Ti-Q3S case due to the wider range of different geometrical arrangements sampled by the silylated Ti(IV) center at finite temperature. The $OSi(CH_3)_3$ group,

pointing outwards the polymeric silica network, is relatively free to move and explore different orientations with respect to the surface. Moreover, in some configurations the "internal" silanol group, also present in Ti-Q3S, is found at hydrogen bond distance from one of the oxygens of the three Ti-O-Si bridges, while in others it points away from the Ti(IV) center and is not involved in hydrogen bonding. Remarkably, the former group of configurations shows a red-shift of the absorption edge (Fig. 11), indicating that weak interactions involving the Ti(IV) site, such as hydrogen bonding, could be responsible of the lower energy threshold of the LMCT transitions.

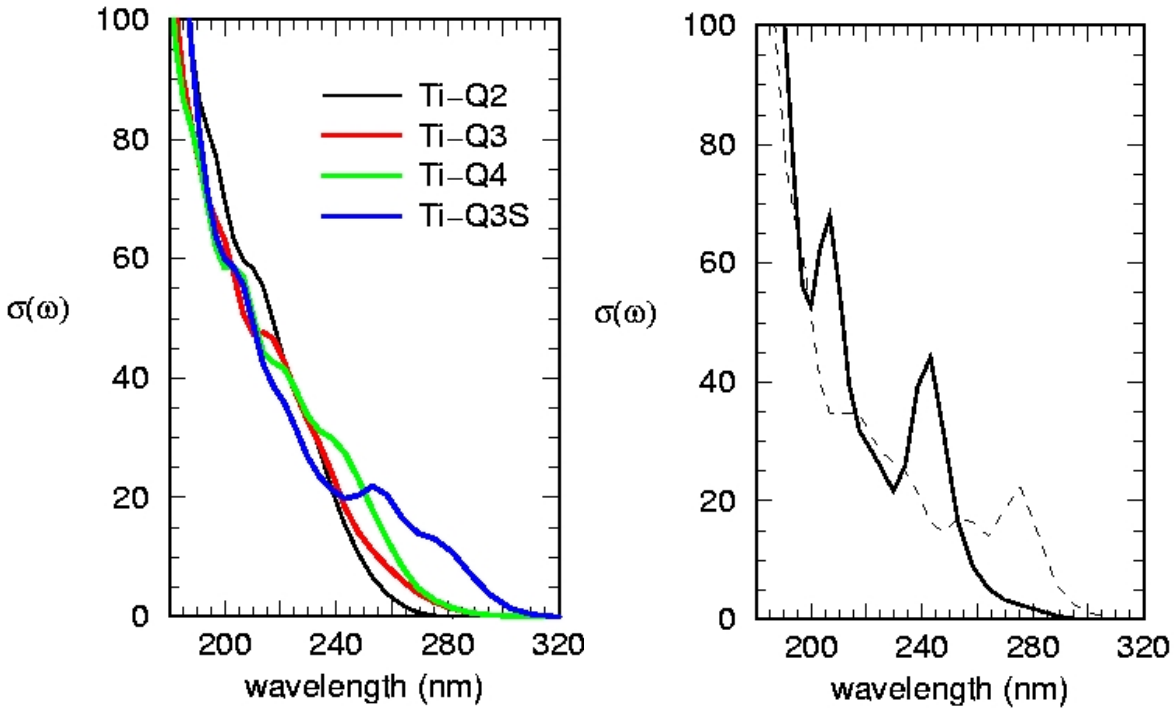

Figure 11. Left panel: Average optical conductivities calculated for the model Ti-containing slabs. Right panel: Contributions of selected configurations to the optical conductivity of Ti-Q3S. The thick solid line represents the contribution of a configuration where no hydrogen bond is present between the Ti-O-Si bridges and the vicinal silanol group. The dashed line refers to a configuration where the silanol is involved in hydrogen bond with Ti-O-Si bridges.

The results of this integrated experimental and theoretical study provide a deeper insight on the properties of Ti(IV)-containing mesoporous silicas through the correlation of the vibrational and electronic features to the microscopic structure of the Ti(IV) center.

The structural details of the Ti(IV) environment have been investigated from first principles simulations of model systems characterized by different types of Ti(IV) sites. In all cases, the average geometry calculated for the Ti(IV) centers was found to be very close to that of an ideal tetrahedron.

Analysis of both experimental and simulated vibrational spectra indicates that the environment of the hydroxyl group affects the OH stretching frequency more than the tetrahedral cation (Ti or Si) to which OH is bonded. This finding further confirms the idea that a detailed interpretation of the high wavenumbers region in IR spectra of Ti(IV)-containing mesoporous silica is indeed not straightforward. In this respect, inspection in the silica window region (1000-800 cm^{-1}) might be helpful in the identification of the vibrational features directly correlated to Ti(IV) centers. In particular, the typical FT-IR band at around 940-930 cm^{-1}, always present in Ti(IV)-samples, is also found in the simulated vibrational spectra at wavenumbers in line with the experimental range and is assigned to Ti-O-X (X= Si or H) asymmetric stretching modes. Such a feature is also responsible of the narrowing of the silica window of Ti(IV)-containing systems with respect to pure silica samples, as indicated by both experimental and simulated spectra. Moreover, this narrowing is also affected by the different structure of the silica matrixes (MCM-41 and MCM-48), in particular it is more pronounced in MCM-41 samples. A further narrowing of the silica window is observed upon silylation, that converts T-OH in T-O-Si$(CH_3)_3$. This finding could be attributed to the replacement of the O-H group with a new kind of tetrahedron (*i.e.* the O-Si-$(CH_3)_3$ group), which also perturbs the vibrational features of the neighboring tetrahedra.

With respect to the main point of this combined investigation, concerning how tripodal Ti(IV) centers could be identified, the simulated vibrational spectra have been of help in the analysis of the experimental FTIR data. Silylation-induced changes in the "silica window" region can be

summarized as follows: quenching of the ~917 cm^{-1} feature, appearance of a shoulder at 942 cm^{-1}, and finally appearance of bands in the 900-880 cm^{-1} range. The first two modifications have been correlated to the chemical transformation of a Ti(IV) tripodal Q3 site to a silylated Ti(IV) center, while features showing up in the low frequency region of the silica window are correlated to the specific O-Si-$(CH_3)_3$ silylated moiety. The finding that the high wavenumbers component inside the silica window region (917 cm^{-1}) of the Ti-Q3 system could be associated to the experimental 930-940 cm^{-1} feature may also explain differences in the FTIR spectra. Indeed in calcined Ti-MCM-48, where tripodal (Q3) Ti(IV) sites are a minor fraction of the total Ti(IV) centers, the intensity of the 930 cm^{-1} component is significantly lower than in calcined Ti-MCM-41, where tripodal sites are the dominant Ti(IV) species.

A detailed analysis of the DR UV-Vis and simulated electronic spectra suggests that the electronic properties of a tripodal Ti(IV) (Ti-Q3), of a silylated Ti(IV) site (Ti-Q3S) and of a tetrapodal site inserted in a model amorphous silica matrix (Ti-Q4) are different for wavelengths longer than 220 nm. In particular, it has been found that the Ti-Q3S model site has peculiar electronic excitation properties, characterized by a depletion of absorption intensity in the 220-240 nm region with respect to the other studied Ti(IV) model systems. This finding is in line with the DR UV-Vis spectra of Ti-MCM-41 and Ti-MCM-48, both characterized by a erosion of the DR profile at ~ 230 nm upon silylation. Such a depletion is also in line with the absorption profile of tetrakis(trimethylsiloxy) titanium,[16] characterized by an intense band at 214 nm and a strong shoulder at 240 nm tailing up to 280 nm.

A detailed analysis of the calculated spectra has also evidenced that small differences in the local environment of the silylated Ti(IV) center might significantly affect the electronic excitation band edge. Such differences could be due to weak interactions involving the Ti(IV) site, for instance with vicinal silanol protons acting as hydrogen bond donors to Ti-O-Si bridges. On the basis of these results, the experimentally observed differences in the DR UV-Vis spectra of Ti-MCM-41 and Ti-MCM-48, where silylation produces a moderate intensity increase in the tail region (250-300 nm)

only in the latter case, may be rationalized by taking into account that the electronic excitation behavior of the Ti(IV) sites can be tuned by the different local environment. As shown in scheme 1, HMDS reacts with two surface OH groups which probably are positioned close to each other, giving in such a case two close silylated sites. In the Ti-Q3S simulation, where only one silylated species is modelled, the O-Si(CH_3)$_3$ group is found to span a large portion of surface due to unhindered rotations of the Ti-O-Si(CH_3)$_3$ bridge around both the Ti-O and O-Si bonds. Such a rotational motion amplitude, which might be dumped in the case of vicinal silylated sites due to steric hindrance, could account for the large variation of the electronic absorption features and edge detected in our calculations and for the different edges experimentally found in silylated Ti-MCM-41 and Ti-MCM-48.

Conclusions

Integrated experimental and simulation approach has proved to be a successful strategy in clarifying the vibrational and electronic properties of different types of Ti(IV) centers and in correlating such properties with the microscopic structure of the active site. In particular, the comparison of both experimental and simulated electronic spectra before and after silylation evidences the presence of Ti-OH groups difficult to detect from the O-H stretching region of IR spectra. However, tripodal Ti(IV) sites can also be associated to the presence of IR bands in the 930-940 cm^{-1} region. The local environment of the Ti(IV) site has proved to be a crucial factor in tuning the observed properties.

Acknowledgements

MURST is acknowledged for financial support (COFIN 2004 - COFIN 2005). Authors are grateful to Compagnia di San Paolo for sponsorship to NIS.

Supporting Information Available: i) FT-IR spectra of Ti-MCM41 in the 2800-3800 cm^{-1} range; ii) calculated vibrational spectra of Ti-Q4 and a Ti-zeolite; iii) calculated partial vibrational spectra for the Ti-Q3S system. This material is available free of charge on the World Wide Web at http://pubs.acs.org.

References and Notes

(1) Corma A. *Chem. Rev.* **1997,** *97*, 2373.

(2) Notari B. *Adv. Catal.* **1996,** *41*, 253.

(3) Oldroyd R.D.; Thomas J.M.; Maschmeyer T.; MacFaul P.A.; Snelgrove D.W.; Ingold K.U.; Wayner D.D.M. *Angew. Chem. Int. Ed.* **1996,** *35*, 2787.

(4) Hu, Y.; Martra G.; Zhang, J.; Higashimoto, S.; Coluccia S.; Anpo, M. *J. Phys. Chem. B* **2006,** *110*, 1680-1685.

(5) Gianotti E.; Dellarocca V.; Marchese L.; Martra G.; Coluccia S.; Maschmeyer T. *Phys. Chem. Chem. Phys.* **2002,** *4*, 6109.

(6) Marchese L.; Maschmeyer T.; Gianotti E.; Coluccia S.; Thomas J.M. *J. Phys. Chem. B* **1997,** *101*, 8836.

(7) Maschmeyer T.; Rey F.; Sankar G.; Thomas J.M. *Nature* **1995,** *378*, 159.

(8) Boccuti M.R.; Rao K.M.; Zecchina A.; Leofanti G.; Petrini G. *Stud. Surf. Sci. Catal.* **1989,** *48*, 133.

(9) Marchese L.; Gianotti E.; Dellarocca V.; Maschmeyer T.; Rey F.; Coluccia S.; Thomas J.M. *Phys. Chem. Chem. Phys.* **1999,** *1*, 585.

(10) Shan Z.; Gianotti E.; Jansen J.C.; Peters J.A.; Marchese L.; Maschmeyer T. *Chem. Eur. J.* **2001,** *7*, 1437.

(11) Raimondi M.E.; Gianotti E.; Marchese L.; Martra G.; Maschmeyer T.; Thomas J.M.; Coluccia S. *J. Phys. Chem. B* **2000,** *104*, 7102.

(12) Jørgensen C.K. *Prog. Inorg. Chem.* **1970,** *12*, 101.

(13) Dellarocca V.; Marchese L.; Peña M.L.; Rey F.; Corma A.; Coluccia S. *Stud. Surf. Sci. Catal.* **2001,** *140*, 209.

(14) Gianotti E.; Dellarocca V.; Peña M.L.; Rey F.; Corma A.; Coluccia S.; Marchese L. *Res. Chem. Inter.* **2004,** *30*, 871.

(15) Dijkgraaf C. *Spectrochim. Acta* **1965,** *21*, 1419.

(16) Fierro L.J.G.; de la Pena O'Shea V.A.Capel-Sanchez M.; Blanco-Brieva G.; Campos-martin J.M. *Angew. Chem. Int. Ed.* **2003,** *42*, 5851.

(17) Fois E.; Gamba A.; Tabacchi G. *ChemPhysChem* **2005,** *6*, 1237.

(18) Fois E.; Gamba A.; Tabacchi G.; Coluccia S.; Martra G. *J. Phys. Chem. B* **2003,** *107*, 10767.

(19) Fois E.; Gamba A.; Tabacchi G.; Coluccia S.; Martra G. *Porous Mat.* **2006,** *in press*.

(20) Corma A.; Kan Q.; Rey F. *Chem. Commun.* **1998,** 579.

(21) Becke, A.D. *Phys. Rev. A* **1988,** *38*, 3098.

(22) Perdew, J.P. *Phys. Rev. B* **1986,** *33*, 8822.

(23) Kleinman, L.; Bylander D. *Phys. Rev. Lett.* **1982,** *48*, 1425.

(24) Troullier, N.; Martins J. *Phys. Rev. B* **1991,** *43*, 1993.

(25) Fois E.; Gamba A. *J. Phys. Chem. B* **1997,** *101*, 4487. (b) Fois E.; Gamba A. *J. Phys. Chem. B* **1999,** *103*, 1794.

(26) (a) Fois E.; Gamba A.; Tabacchi G. *J. Phys. Chem. B* **1998,** *102*, 3974. (b) Fois E.; Gamba A.; Tabacchi G. *Phys. Chem. Chem. Phys.* **1999,** *1*, 531. (c) Fois E.; Gamba A.; Tabacchi G. *Stud. Surf. Sci. Catal.* **1999,** *125*, 285.

(27) (a) Fois E.; Gamba A.; Tabacchi G. *Chem. Phys. Lett.* **2000,** *329*, 1. (b) Fois E.; Gamba A.; Tabacchi G. *Stud. Surf. Sci. Catal.* **2001,** *140*, 251.

(28) (a) Fois E.; Tabacchi G.; Quartieri S.; Vezzalini G. *J. Chem. Phys*. **1999**, *111*, 355. (b) Fois E.; Gamba A.; Tabacchi G.; Quartieri S.; Vezzalini G. *J. Phys. Chem. B* **2001,** *105*, 3012. (c) Fois E.; Gamba A.; Tabacchi G.; Quartieri S.; Vezzalini G. *Phys. Chem. Chem. Phys*. **2001**, *3*, 4158.

(29) (a) Ferro O.; Quartieri S.; Vezzalini G.; Fois E.; Gamba A.; Tabacchi G. *Am. Mineral.* **2002**, *87*, 1415. (b) Ceriani C.; Fois E.; Gamba A.; Tabacchi G.; Ferro O.; Quartieri S.; Vezzalini G. *Am. Mineral.* **2004,** *89*, 102. (c) Fois E.; Gamba A.; Tabacchi G.; Arletti R.; Quartieri S.; Vezzalini G. *Am. Mineral.* **2005,** *90*, 28.

(30) Fois E.; Gamba A.; Spanò E.; Tabacchi G. *J. Mol. Struct.* **2003,** *644*, 55.

(31) Fois E.; Gamba A.; Spanò E. *J. Phys. Chem. B* **2004,** *108*, 154.

(32) Fois E.; Gamba A.; Spanò E. *J. Phys. Chem. B* **2004,** *108*, 9557.

(33) Spanò E.; Tabacchi, G.; Gamba, A.; Fois, E. *J. Phys. Chem. B* **2006,** *in press.*

(34) Car R.; Parrinello M. *Phys. Rev. Lett.* **1985,** *55* (2471).

(35) CPMD code ver 3.9 *Copyright IBM corp 1990-2006, copyright MPI fuer Festkoerperforschung Stuttgart 1997-2001, www. cpmd. org* **2006**.

(36) Marx, D.; Hutter, J; In *Modern Methods and Algorithms of Quantum Chemistry*, Vol. 1; Grotendorst, J., Ed.; Forschungzentrum Julich: Julich, D, **2000**.

(37) Van Beest B.W.H.; Kramer G.J.; van Santen R.A. *Phys. Rev. Lett.* **1990,** *64*, 1955.

(38) Madden P.A. *In Liquids, Freezing and Glass Transition Hansen, J. P. Levesque, D. Zinn-Justin, J. , Eds. Elsevier Science: London, UK* **1991**.

(39) Bassani F.; Pastori Parravicini G. *Electronic States and Optical Transitions in Solids Pergamon Press: Oxford* **1975**.

(40) Fois E.; Selloni A.; Parrinello M. *Phys. Rev. B* **1989,** *39*, 4812.

(41) Vartuli J.C.; Schmitt K.D.; Kresge C.T.; Roth W.J.; Leonowicz M.E.; McCullen S.B.; Hellring S.D.; Beck J.S.; Schlenker J.L.; Olson D.H.; Sheppard E.W. *Chem. Mater.* **1994,** *6*, 2317.

(42) Kresge C.T.; Leonowicz M.E.; Roth W.J.; Vartuli J.C.; Beck J.S. *Nature* **1992,** *359*, 710.

(43) de Man A.J.M.; Sauer J. *J. Phys. Chem.* **1996,** *100*, 5025.

(44) Morrow B.A.; McFarlan A.J. *J. Phys. Chem.* **1992,** *96*, 1395.

(45) Zecchina A.; Bordiga S.; Spoto G.; Marchese L.; Petrini G.; Leofanti G.; Padovan M. *J. Phys. Chem.* **1992,** *96*, 4991.

(46) Bolis V.; Bordiga S.; Lamberti C.; Zecchina A.; Carati A.; Rivetti F.; Spanò G.; Petrini G. *Langmuir* **1999,** *15*, 5753.

(47) Peña M.L.; Dellarocca V.; Rey F.; Corma A.; Coluccia S.; Marchese L. *Micropor. Mesopor. Mater.* **2001,** *44-45*, 345.

(48) Casida M.E.; Jamorsky C.; Casida K.C.; Salahub D.R. *J. Chem. Phys.* **1998,** *108*, 4439.